End-to-End Noise Model for Intra-Body Terahertz Nanoscale Communication

Hadeel Elayan, *Student Member, IEEE*, Cesare Stefanini, *Member, IEEE*, Raed M. Shubair, *Senior Member, IEEE*, and Josep Miquel Jornet, *Member, IEEE*

***Abstract*— *In vivo* wireless nanosensor networks (iWNSNs) are paving the way toward transformative healthcare solutions. These networks are expected to enable a plethora of applications, including drug-delivery, bio-sensing, and health monitoring. With the development of miniature plasmonic signal sources, antennas, and detectors, wireless communications among intrabody nanodevices will expectedly be enabled in the terahertz (THz) frequency band (0.1–10 THz). Several propagation models were recently developed to analyze and assess the feasibility of intra-body electromagnetic (EM) nanoscale communication. The emphasis of these works has mainly been on understanding the propagation of EM signals through biological media, with limited focus on the intra-body noise sources and their impact on the system performance. In this paper, a stochastic noise model for iWNSNs is presented in which the individual noise sources that impact intra-body systems operating in the THz frequency band are analyzed. The overall noise contributions are composed of three distinctive constituents, namely, Johnson–Nyquist noise, black-body noise, and Doppler-shift-induced noise. The probability distribution of each noise component is derived, and a comprehensive analytical approach is developed to obtain the total noise power-spectral density. The model is further validated via 2-D particle simulations as the active transport motion of particles is conveyed in the presented framework. The developed models serve as the starting point for a rigorous end-to-end channel model that enables the proper estimation of data rate, channel capacity, and other key parameters, which are all factors of the noise environment.**

***Index Terms*— Nanonetworks, terahertz band, noise model, intra-body.**

Manuscript received May 17, 2018; revised July 26, 2018; accepted August 29, 2018. Date of publication September 6, 2018; date of current version November 16, 2018. This work was supported in part by the Information and Communications Technology (ICT) Fund in United Arab Emirates and in part by the U.S. National Science Foundation (NSF) under Grant IIP-1718177 and Grant CBET-1706050. *(Corresponding author: Hadeel Elayan.)*

H. Elayan and C. Stefanini are with the Healthcare Engineering Innovation Center, Department of Biomedical Engineering, Khalifa University, Abu Dhabi 127788, United Arab Emirates (e-mail: hadeel.mohammad@ku.ac.ae; cesare.stefanini@ku.ac.ae).

R. M. Shubair is with the Research Laboratory of Electronics, Massachusetts Institute of Technology, Cambridge, MA 02139 USA (e-mail: rshubair@mit.edu).

J. M. Jornet is with the Department of Electrical Engineering, University at Buffalo, The State University of New York, Buffalo, NY 14260 USA (e-mail: jmjornet@buffalo.edu).

Digital Object Identifier 10.1109/TNB.2018.2869124

I. Introduction

THE future of healthcare is dramatically progressing with the acceleration of medical technologies. The strive towards miniaturization is creating innovative solutions that would ensure better effectiveness in diagnosis and treatments. Such aspiration is correlated with an intense evolution in the field of nanotechnology and in the development of micro/nano-scale robotic systems. Magnetic nano-swimmers [1], bacteria-powered microrobots [2], and ant-like nano-engines [3] are few examples of biologically-inspired nanomachines. In parallel to these advancements, the growth witnessed in the fields of nano-electronics, nano-plasmonics and nano-photonics is expediting the development of nanosensors that are capable of detecting different events with unprecedented sensing and actuation capabilities. Among others, plasmonic nano-lasers with sub-micrometric footprint [4], plasmonic nano-antennas able to confine light in nanometric structures [5] and single-photon detectors with unrivaled sensitivity [6] have already been developed. Eventually, the aforementioned progress in the various domains have paved the way towards in-vivo wireless nanosensor networks (iWNSNs). These networks have been recently proposed as a technique to provide faster and more precise disease diagnosis and treatments in comparison to traditional technologies [7].

Both molecular and electromagnetic (EM) communications are leading wireless technologies that could enable communication between nanomachines. On the one hand, although molecular communication is being thoroughly investigated [8], it suffers from low achievable data rates which drastically limit the usefulness of nanosensor networks. On the other hand, from an EM perspective, plasmonic nano-antennas have enabled wireless communication among nano-devices at high frequencies, ranging from the Terahertz (THz) band (0.1-10 THz) to the optical frequency bands (infrared, 30-400 THz, and visible, 400-750 THz).

The study of the THz band propagation within the human body is still at its infancy as most nano-biosensing applications rely on the use of light. Numerical analysis and characterization of THz propagation through various body tissues have been presented in [9]–[11]. A genuine model that accounts for the intra-body signal degradation has been presented in [12]. A complementary multi-layer intra-body

model for nano-biosensing applications can be found in [13]. Alternatively, Johari and Jornet [14] advocated for the use of the optical window for intra-body wireless communication among nanosensors with plasmonic nano-antennas. Starting from these, the development of comprehensive architectures and protocols for intra-body nanonetworks comprise the path of research that ought to be addressed.

One of the most important metrics that should be studied to assess the quality of any communication system is noise. Basically, noise degrades the signal transmission quality and affects the system throughput as it may impose re-transmission of data packets or extra coding to recover data in the presence of errors. Nevertheless, the proper characterization of noise is one of the main challenges in the information theoretical analysis of intra-body EM nanocommunication. Current research in the literature which considers noise in the THz frequency band can be found in [6] and [15]. Yet, in the framework of in-vivo wireless networks, few works exist to study this fundamental parameter which should be analyzed in order to accurately evaluate the in-vivo communication link [16], [17]. Particularly, small systems, as found in molecular biology and in the drive toward miniaturization [18] can show strong susceptibility to noise. In our recent previous work, a deterministic thermal noise analysis for intra-body communication based on the diffusive heat flow theory has been developed [19].

In this work, we present a novel stochastic noise model for intra-body wireless communications in the THz frequency band. We classify the three main noise sources inside the body, which include the Johnson-Nyquist noise, Black-body noise, as well as Doppler-shift-induced noise. The underlying physical fundamentals of each noise source are comprehensively explained. Moreover, the probability distribution of each noise component is derived and a complete noise model is developed, allowing to compute the total noise power-spectral density of the in-vivo medium in the THz frequency band. It is important to note that these noise sources basically arise due to the fluctuation of particles, which occurs either naturally or gets triggered upon exposure to EM radiation. Therefore, to validate our model, we perform two-dimensional particle simulations, where multiple particle tracks are generated. Random displacements are simulated to enable analysis of the particle motion, allowing appropriate verification of the analytical framework. The significance of the presented study lies in providing an understanding of the intrinsic limits of intra-body communication in the THz frequency band. It results in a realistic evaluation of iWNSNs and opens the door towards developing techniques which maximize the efficiency of such communication link. Thereafter, data rate, maximum transmit power, maximum transfer receiver distance as well as channel capacity could be all properly estimated as they are factors of the noise environment.

The rest of the paper is organized as follows. In Sec. II, a characterization of the intra-body medium in the THz frequency band is illustrated. In Sec. III, the different intra-body noise sources, namely, the Johnson noise, Black-body noise, as well as the Doppler- shift-induced noise are presented. In Sec. IV, the mathematical framework of each noise source is established. In Sec. V, both numerical and simulation results of the developed noise models are demonstrated. Finally, we draw our conclusions in Sec. VI.

II. Characterization of Intra-Body Communication

In order to be capable of developing the noise model, a proper characterization of the intra-body medium is necessitated. Such characterization is attained upon computing a number of interrelated parameters including the medium permittivity, index of refraction, absorption cross section as well as temperature increase. In fact, as size goes down to the nanoscale, the physical and electrical properties of materials change, and novel properties arise in the matter. Such impact can be beneficial if harnessed properly. In light of our research, electrical properties of tissues in the THz frequency must be accounted for when studying intra-body communication.

The scale that we are operating at is referred to as the "mesoscopic" length scale, which is intermediate between the molecular and macroscopic scales. At the THz frequency band, the disordered nature and microstructure of biological matter as well as the supra-cellular organization in such materials trigger different polarization mechanisms which include multiple relaxation times and non-symmetric time-domain responses [20]. In specific, the dielectric response in the frequency domain of tissues having high water content can be characterized by the Debye Relaxation Model [21]. This model describes the reorientation of molecules that could involve translational and rotational diffusion, hydrogen bond arrangement, and structural rearrangement. For a pure material, multiple Debye processes are possible where the complex permittivity is described by [22]

$$\epsilon(\omega) = \epsilon_\infty + \sum_{j=1}^{n} \frac{\Delta\epsilon}{1 + j\omega\tau_j}, \tag{1}$$

in which ϵ_∞ is the permittivity at the high frequency limit, $\Delta\epsilon = \epsilon_j - \epsilon_{j+1}$, ϵ_j are intermediate values, occurring at different times of the permittivity, τ_j is the relaxation time relating to the j^{th} Debye type relaxation process, and ω is the angular frequency given as $2\pi f$.

Biological tissues are principally an assembly of biological cells, each with different sub-cellular components that exhibit different responses and relaxation times. To provide the best approximation of complex permittivity for polar liquids at frequencies in the lower THz band, the double Debye equations are used [23]

$$\epsilon(\omega) = \epsilon_\infty + \frac{\epsilon_1 - \epsilon_2}{1 + j\omega\tau_1} + \frac{\epsilon_2 - \epsilon_\infty}{1 + j\omega\tau_2}. \tag{2}$$

Equation (2) is rationalized and the real and imaginary parts of the complex permittivity are separated as follows

$$\epsilon'(\omega) = \epsilon_\infty + \frac{\epsilon_1 - \epsilon_2}{1 + (\omega\tau_1)^2} + \frac{\epsilon_2 - \epsilon_\infty}{1 + (\omega\tau_2)^2}, \tag{3}$$

$$\epsilon''(\omega) = \frac{(\epsilon_1 - \epsilon_2)(\omega\tau_1)}{1 + (\omega\tau_1)^2} + \frac{(\epsilon_2 - \epsilon_\infty)(\omega\tau_2)}{1 + (\omega\tau_2)^2}. \tag{4}$$

TABLE I
PERMITTIVITY AND RELAXATION TIME VALUES FOR VARIOUS MEDIA

Model	ϵ_∞	ϵ_1	ϵ_2	τ_1(ps)	τ_2(ps)
Water [24]	3.3	78.8	4.5	8.4	0.1
Blood [24]	2.1	130	3.8	14.4	0.1
Skin [21]	3.0	60.0	3.6	10.0	0.2
Fat [25]	3.0	60.0	3.6	10.0	0.2

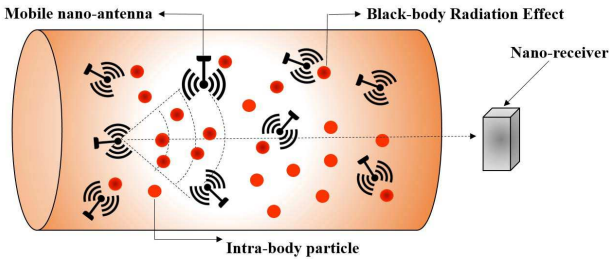

Fig. 1. Intra-body system model composed of various intra-body particles, mobile nano-antennas, and a nano-receiver.

Using the values in Table I, $\epsilon'(\omega)$ and $\epsilon''(\omega)$ can be computed for the different intra-body media. These values are used then to calculate the effective index of refraction as

$$n(\omega) = \sqrt{\frac{\sqrt{\epsilon'^2(\omega) + \epsilon''^2(\omega)} + \epsilon'(\omega)}{2}}. \quad (5)$$

It is important to note that the imaginary part of the index of refraction is utilized in the computation of the particles absorption cross section [12], which is an integral part of computing the effective medium temperature as clearly explained in [19].

III. INTRA-BODY NOISE CLASSIFICATION

Our system of interest is composed of a medium full of both biological cells as well as liquid-surrounded heat sources larger than tens of nanometers (nm), as illustrated in Fig. 1. The heat sources in this work are considered to be nano-antennas in nano-biosensing implants in the human body. Nano-biosensors have the capability to detect the minutest interacting phenomenon, which enables a far greater and much reliable degree of estimation of biological interactions [26]. Throughout this paper, we will use the general term "particle" to refer to both the biological cells and the nano-antennas. As the nano-antennas radiate EM waves, cells will capture part of this EM energy through the process of molecular absorption. The absorbed EM energy will be converted into heat which will result in temperature increase around the cells, as has been extensively discussed by Elayan *et al.* [19]. Hence, subsequent to such exposure, the cells also become heat sources. Fundamentally, temperature is a key factor in computing the noise associated with a communication system.

In this scenario, we identify three noise sources: Johnson noise, Black-body noise and the Doppler-shift-induced noise. Johnson noise exists as a result of the detecting nano-receiver at the receiver side. Black-body noise arises as a natural contribution of the thermal EM radiation within or surrounding a body. In the case of the Doppler-shift-induced noise, the propagation between the nano-receiver is not only by a direct line-of-sight route, but via many paths as different scatterers change the plane waves incident on the receiver. Consequently, the received signal at any point consists of a large number of horizontally travelling uniform plane waves whose amplitudes, phases and angles of arrival have each a random component.

IV. INTRA-BODY NOISE ANALYSIS

In this section, a comprehensive analysis of the identified noise sources is presented.

A. Johnson-Nyquist Noise

Within every communication system, particularly at the front-end, components that contribute noise to the detection process exist. This results in degrading the ultimate detectability of the signal. The majority of this noise arises from electronics, particularly mixers or direct detectors as well as transistors in amplifiers that follow these devices [27]. Thermal noise, also referred to as Johnson-Nyquist noise, is produced by fluctuations of charged particles (usually electrons) in conducting media [28]. Any component in the system that dissipates power generates thermal noise. When a resistor R, is at temperature T, random electron motion produces noise voltage, $V(t)$, at the open terminals. Consistent with the central limit theorem, $V(t)$ has a Gaussian distribution with an rms voltage of [28]

$$V_{rms} = \sqrt{4k_b T R B}, \quad (6)$$

where k_b is Boltzmann constant, h is Planck constant and B is the bandwidth of the measuring system. The probability density function (PDF) of the noise voltage, V_{rms}, is given by

$$p(x) = \frac{1}{V_{rms}\sqrt{2\pi}} \mathbf{exp}\left(-\frac{x^2}{2V_{rms}^2}\right). \quad (7)$$

The theory further shows that the mean square spectral density of thermal noise is [28]

$$G_v(f) = 2Rhf \cdot \mathbf{exp}\left[-\left(\frac{hf}{k_b T} - 1\right)\right]. \quad (8)$$

Instead of dealing with mean square voltage, the available spectral density at the load resistance could be found using the maximum power transfer theorem as

$$G_a(f) = \frac{G_v(f)}{4R}. \quad (9)$$

Thus, the first source of noise that is always found in an in-vivo wireless communication system arises from the thermal cycle of heat exchange between the receiver, which is a nano-antenna in our assumed scenario, and the environment. It is to be noted that the Gaussian distribution of the Johnson Nyquist noise is developed on the basis of a model detector containing a very large number of independent receivers which produce an infinitesimal contribution to the resultant amplitude. The convolution of a large number of elementary distributions approaches a Gaussian distribution even though the elementary distributions themselves maybe non-Gaussian

and all different. In addition, one must remember that the distribution of a thermally excited mode is the result of a large number of independent statistical forces acting on it at random. The resonant mode model was chosen in order to easily integrate the quantum effects in the analysis [29].

B. Black-Body Noise

Every physical body spontaneously and continuously emits EM radiation. The emitted radiation is described by Planck's law [30]. The higher the temperature of a body, the more radiation it emits at every wavelength. Due to the EM radiation of nano-antennas, the human body particles will seize part of the EM energy. As a result, the absorbed power will activate the vibration of the particles, which will result in heat generation and temperature increase. The intra-body medium could be denoted as a black-body since it is associated with temperature above absolute zero. Therefore, the intra-body channel always has background noise even without signal transmission.

The spectral radiance of a body, E_f, describes the amount of energy it gives off as radiation of different frequencies. It is measured in terms of the power emitted per unit area of the body, per unit solid angle that the radiation is measured over, per unit frequency as [31]

$$E_f(f,T) = \frac{2hf^3}{c^2}\mathbf{exp}\left[-\left(\frac{hf}{k_bT}-1\right)\right], \tag{10}$$

where c is the speed of light in the medium. The power spectral density, $H(f)$, is the product of the spectral radiance, $E_f(f,T)$, and the effective aperture area, A_{eff}, of the nano-antenna, i.e.

$$H(f) = E_f(f,T)A_{eff}, \tag{11}$$

where A_{eff} is inferred from the amount of noise that the antenna intercepts and is given by

$$A_{eff} = \frac{\lambda_g^2}{4\pi}. \tag{12}$$

λ_g is the effective wavelength given as λ/n', where n' and n'' are the real and imaginary parts of the tissue refractive index n, respectively. The tissue refractive index provided in (5) can be written as

$$n = n' - jn''. \tag{13}$$

In classical physics, black-body radiation is considered as chaotic EM radiation. The average spatial distribution of such stationary radiation is homogeneous and isotropic, where the electric field strength and the magnetic induction of its spectral components have completely random amplitudes built up of infinitely many independent, infinitesimal contributions [32], [33]. In this description, the electric field strength and the magnetic induction of a mode are proportional with the random processes, in which their amplitudes have a Gaussian density function based on the central limit theorem [34]. As such, both the electric field and the magnetic induction of a mode of the thermal radiation (in a small spatial region) have a Fourier series representation given by [32], [35]

$$x(t) = \frac{1}{2}a_0 + \sum_{n=1}^{N} a_n\mathbf{cos}(2\pi f_n t) + b_n\mathbf{sin}(2\pi f_n t). \tag{14}$$

Thereby, the phenomenon is described by a characteristic set of frequencies or modes, f_n. If we take a particular mode of the radiation field, a_n as an example, we have [35]

$$a_n = \frac{2}{T}\int_0^T x(t)\mathbf{cos}(2\pi f_n t)dt. \tag{15}$$

Next, we consider the characteristic function of this particular mode given as

$$\varphi_n(A) = \left\langle e^{-ja_nA}\right\rangle. \tag{16}$$

The term $\langle a_n^2\rangle$ is related to the correlation function by

$$\left\langle a_n^2\right\rangle = \frac{4}{T^2}\int_0^T\int_0^T \left\langle x(t')x(t'')\right\rangle \mathbf{cos}\omega_n t'\mathbf{cos}\omega_n t''dt'dt''. \tag{17}$$

Using the properties of a Gaussian random process, it is known that

$$\left\langle x(t')x(t'')\right\rangle = 2D\delta(t'-t''), \tag{18}$$

in which D refers to the translational diffusion coefficient. In our case, this is given by

$$D = \frac{k_bT}{\zeta}. \tag{19}$$

The parameter, ζ, is a friction coefficient which is going to be defined in the subsequent section. It then follows that [35]

$$\langle\mathbf{exp}(-ja_nA)\rangle = \mathbf{exp}\left[-\frac{1}{2}A^2\left\langle a_n^2\right\rangle\right], \tag{20}$$

where

$$\left\langle a_n^2\right\rangle = \frac{4D}{T}. \tag{21}$$

The probability that a_n^2 has a particular value of a_n follows from the Fourier transform, and the form of the characteristic function indicates that the distribution is Gaussian. The PDF of the excitation of the amplitude, a_n, is given by [35]

$$p(a_n) = \frac{1}{\langle a_n\rangle}\sqrt{2\pi}\,\mathbf{exp}\left[-\frac{a_n^2}{2\langle a_n^2\rangle}\right]. \tag{22}$$

C. Doppler-Shift-Induced Noise

The internal fluctuations which result from the heat transfer mechanism experienced by the intra-body system are characterized by the cells' random and irregular velocity. In fact, the erratic motion of suspended particles, referred to as the Brownian motion, deals with mesoscopic dynamics, which are ubiquitous in the micro and nano-world, and in particular in soft and biological matter [36].

To assess such scenario, consider the one-dimensional motion of a spherical particle with radius r, mass m, position x, and velocity $v(t)$ in a fluid medium having a viscosity η. Newton's equation of motion for the particle is [37]

$$m\frac{dv(t)}{dt} = F_{tot}(t), \tag{23}$$

where $F_{tot}(t)$ is the total instantaneous force on the particle at time t, arising from the interaction of the particle with the surrounding medium. This force is governed by a friction force, F_{fric}, proportional to the velocity, $v(t)$, of the particle and given as [38]

$$F_{fric} = -\zeta v(t), \tag{24}$$

where the friction coefficient, ζ, also referred to as the drag constant, is described by Stokes law as [37]

$$\zeta = 6\pi\eta r. \tag{25}$$

A random force, $\xi(t)$, represents the rapidly fluctuating part of F_{tot}. For such scenario, the analysis could be modeled using the Brownian particle equations of motion, referred to as *Langevin equations*, given by [38]

$$\begin{aligned} m\frac{dv(t)}{dt} &= -\zeta v(t) + \xi(t), \\ \frac{dv(t)}{dt} &= -\gamma v(t) + \frac{1}{m}\xi(t), \end{aligned} \tag{26}$$

where $\gamma = \zeta/m$. The force during an impact is supposed to vary with extreme rapidity over the time of any observation, i.e. in any infinitesimal time interval, which cannot be strictly true in any real system. Therefore, the effect of the fluctuating force can be illustrated by providing its first and second moments as time averages over infinitesimal time interval [39]

$$\langle\xi(t)\rangle_\xi = 0, \quad \langle\xi(t_1), \xi(t_2)\rangle_\xi = 2\beta\delta(t_1 - t_2), \tag{27}$$

where $\langle ...\rangle_\xi$ is an average with respect to the distribution of the realizations of the stochastic variable $\xi(t)$, and β is a measure of the strength of the fluctuation force. If $\xi(t)$ is continuous, the existence of a local solution for (26) is guaranteed. An explicit formal solution of (26) can be obtained as [38]

$$v(t) = v(0)e^{-\gamma t} + \frac{1}{m}\int_0^t e^{-\gamma(t-x)}\xi(x)dx, \tag{28}$$

where $v(0)$ is the initial velocity of the medium constituents. The mean squared velocity can be found from (28) as [39]

$$\left\langle v(t)^2 \right\rangle = v(0)^2 e^{-2\gamma t} + \frac{\beta}{\zeta m}(1 - e^{-2\gamma t}). \tag{29}$$

In the long time limit, the exponential drops out and the mean squared velocity must approach its equilibrium value k_bT/m. Consequently, we have [39]

$$\beta = \zeta k_b T. \tag{30}$$

The changing velocity of the source (nano-antennas in nano-biosensing implants in the human body) results in Doppler-shifts to the transmitted frequency of light originating from a source that is moving in relation to the observer (receiver). Therefore, the wave is observed to have frequency, f_d, for a signal arriving at an angle, ϕ, given as

$$f_d = f_m \mathbf{cos}\phi, \tag{31}$$

where

$$f_m = \frac{\langle v(t)\rangle}{\lambda_g}. \tag{32}$$

is the maximum Doppler-shift at the particle speed and carrier wavelength, λ_g.

The received signal $R(f, t)$ is a result of many plane waves each shifted by the Doppler contribution appropriate to the particle motion relative to the direction of the plane wave [40]. The power contributed to the received signal by plane waves constitutes of the power, $f(\phi)d(\phi)$, arriving in the angular interval that would be received by an isotropic nano-antenna of the same polarization, multiplied by the nano-antenna gain, $G(\phi - \alpha)$, multiplied by the square of the parallel fraction of polarization $\left[p_u(\phi) \cdot p_g(\phi - \alpha)\right]$ as [41]

$$f(\phi)d(\phi)\left[p_u(\phi) \cdot p_g(\phi - \alpha)\right]^2 G(\phi - \alpha). \tag{33}$$

From (32), we find $d\phi$ as

$$d\phi = -\frac{1}{f_m\sqrt{1 - \left(\frac{f_d}{f_m}\right)^2}}df. \tag{34}$$

By substituting (34) into (33) and combining the two angles ($\stackrel{+}{-}\phi$) from which the Doppler-shift, f_d arises, the power-spectral density of $R(f, t)/\sqrt{2}$ is given as [40]

$$S(f) = S_1(f) + S_2(f), \tag{35}$$

in which

$$S_1(f) = \frac{f(\phi)G(\phi - \alpha)\left[p_u(\phi) \cdot p_g(\phi - \alpha)\right]^2}{f_m\sqrt{1 - (f_d/f_m)^2}}, \tag{36}$$

and

$$S_2(f) = \frac{f(-\phi)G(-\phi - \alpha)\left[p_u(-\phi) \cdot p_g(-\phi - \alpha)\right]^2}{f_m\sqrt{1 - (f_d/f_m)^2}}, \tag{37}$$

where $\phi = \left|\mathbf{cos}^{-1}\frac{f_d}{fm}\right|$. Similar to mobile-radio reception, both the in-phase and quadrature components at any given time, t, are independent Gaussian random variables with the following PDF [40]

$$f(x) = \frac{1}{\sigma\sqrt{2\pi}}\mathbf{exp}\left[-\frac{x^2}{2\sigma^2}\right]. \tag{38}$$

x in this case is the in-phase component of $R(f, t)$ and σ is the RMS value given as

$$\sigma = \sqrt{\int_{-f_m}^{f_m} S(f)df}. \tag{39}$$

As the body is composed of a large number of cells, particles, etc., the number of received plane waves and thus multipath components is large. Thereby, the central limit theorem is utilized to indicate that the channel response mimics a Gaussian process. As such, since Doppler shift noise is dependent on signal transmission, this noise element follows a Gaussian distribution.

D. Combined Noise Model

In order to formulate an end-to-end noise model, the total noise power spectral density should be calculated. From the analysis presented above, it is clear that the three noise sources are probabilistically independent. Thereafter, the resulting PDF is the convolution of (7), (22) and (38). As we are dealing with three Gaussian PDFs, we should recall that the convolution of Gaussian functions is also a Gaussian, with variance being the sum of the original variances [42]. This can be proved by knowing that the Fourier transform of a Gaussian, $f_X(x) = \mathcal{N}(x; \mu_X, \sigma_X^2)$ is given as

$$F\{f_X\} = F_X(\omega) = \mathbf{exp}[-j\omega\mu_X]\mathbf{exp}[-\frac{\sigma_X^2\omega^2}{2}]. \quad (40)$$

According to the convolution theorem and by considering three Gaussian PDFs we have

$$\begin{aligned} f_Z &= f_X * f_Y * f_W = \mathcal{F}^{-1}\{\mathcal{F}\{f_X\} \cdot \mathcal{F}\{f_Y\} \cdot \mathcal{F}\{f_Z\}\} \\ &= \mathcal{F}^{-1}\Bigg\{\mathbf{exp}\left[-j\omega\mu_X\right]\mathbf{exp}\left[-\frac{\sigma_X^2\omega^2}{2}\right]\mathbf{exp}\left[-j\omega\mu_Y\right] \\ &\quad \times \mathbf{exp}\left[-\frac{\sigma_Y^2\omega^2}{2}\right]\mathbf{exp}\left[-j\omega\mu_W\right]\mathbf{exp}\left[-\frac{\sigma_W^2\omega^2}{2}\right]\Bigg\} \\ &= \mathcal{F}^{-1}\Bigg\{\mathbf{exp} - j\omega\left(\mu_X + \mu_Y + \mu_W\right) \\ &\quad \times \mathbf{exp}\left[-\frac{\left(\sigma_X^2 + \sigma_Y^2 + \sigma_W^2\right)\omega^2}{2}\right]\Bigg\} \\ &= \mathcal{N}(z; \mu_X + \mu_Y + \mu_W). \end{aligned} \quad (41)$$

To compute the total power spectral density, we add the spectral densities of the individual noise sources. To do so, we consider the simplest nano-antenna structure demonstrated to date, i.e., a nano-dipole antenna, with $G(\alpha) = 1.5$. By substituting the gain of the antenna, (35-37) will lead to

$$S_{sim}(f) = \frac{3}{f_m\sqrt{1 - \left(\frac{f_d}{f_m}\right)^2}}. \quad (42)$$

Next, we sum of the individual noise contributors in the in-vivo system as

$$N_{tot}(f) = G_a(f) + H(f) + S_{sim}(f). \quad (43)$$

V. Simulation Results

In this section, we evaluate and validate the intra-body noise model presented in Sec. IV using MATLAB©. We follow a model that assumes a homogeneous medium of identical particles. Note that a biological tissue is an ensemble of similar cells having the same origin, where together with other tissues, it forms an organ. In intra-body communications, the EM wave will pass through a structured layer of different tissues, namely, the organ (e.g., the skin which contains different layers). Therefore, to find out the EM intensity in each layer, the need for a non-homogeneous model is clear [43]; however, once the EM intensity is given in a specific region (tissue), then the homogeneous assumption for the noise analysis can be adopted. As mentioned in Sec. III, the primary energy source in the system is a nano-antenna, which radiates an EM wave at a distance. As a result of the absorption, cells become heat sources.

TABLE II
Simulation Parameters

Parameter	Symbol	Unit	Value	Ref.
Red blood cell radius	r	m	4×10^{-6}	[49]
Red blood cell mass	m	pg	33	[50]
Red blood cell viscosity	η	Pa·s	0.00278	[51]
Initial cell velocity	$v(0)$	mm/s	1.1	[48]

In this paper, we provide numerical results for the specific case of red blood cells (RBCs), where in our scenario blood is assumed to be composed of RBCs immersed in homogeneous plasma. It is to be noted that the characterization of RBCs based on the Doppler shift holds true as RBCs resemble Rayleigh scatterers that experience single or multiple relaxations. As such, the RBCs velocity profiles are impacted resulting in a novel measure of their propagation capability [44]. In addition, RBCs represent black body elements, which impact the entire medium they are suspended in. Such assumption holds even before the exposure of RBCs to EM radiation. Indeed, between the outer surface of the cell membrane and the inner contents of the cell there is always the electric potential difference, which is stimulated due to both the different concentrations of K+, Na+ and Cl- inside and outside of the cell as well as their different permeability through the cell membrane [45]. Upon excitation, a living cell changes the membrane electric potential because of changes in the membrane permeability and active ion movement through the membrane. Thus, owing to the bioelectret condition of certain subcellular structures in the cell and its surroundings, a slowly oscillating electric field that is strong enough to influence the biological processes is generated [46]. Further, the examination of RBCs allows the identification of health disorders. In particular, several blood diseases involve modification in the morphology of such cells, including, sickle-cell disease, malaria and spherocytosis. For these reasons, many non-invasive optical imaging systems have been developed for the investigation of RBC morphology as a diagnostic clinical factor [47].

In our analysis, we utilize realistic parameters of RBCs as given in Table II. These parameters play a fundamental role in calculating the various noise constituents including finding the temperature [19], drag constant, translational diffusion coefficient, mean squared velocity ..etc. Such dependence clearly indicates that our study relates the intra-body medium to the presented noise analysis. Fig. 2 provides a visualization of the propagation scenario of RBCs in which the velocity profile of these particles changes as they propagate in the body, upon being stimulated by a nanoantenna. The initial velocity of RBCs can be obtained via experimental measurements from the literature as provided in [48]. As such, the mean squared velocity can be computed from which the Doppler shift induced noise is calculated as presented in (29) and (32).

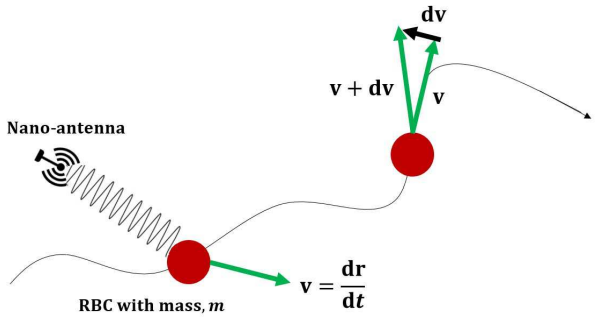

Fig. 2. A visualization of the propagation scenario of excited RBCs, where the velocity profile of the cells change as they propagate through the body.

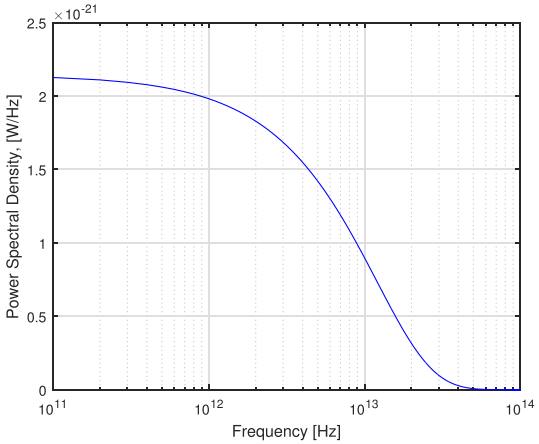

Fig. 3. Johnson-Nyquist noise power spectral density at the high frequency regime including the THz frequency band.

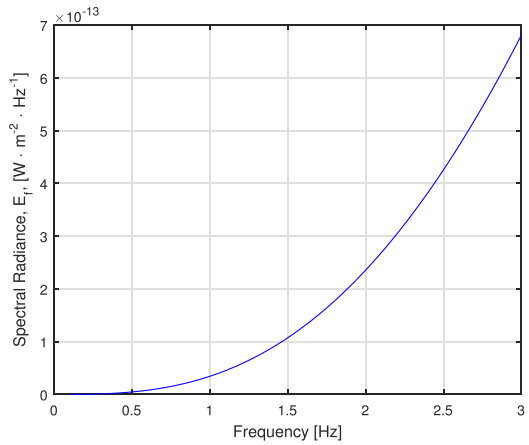

Fig. 4. Black-body noise power spectral density of an intra-body medium at the THz frequency band.

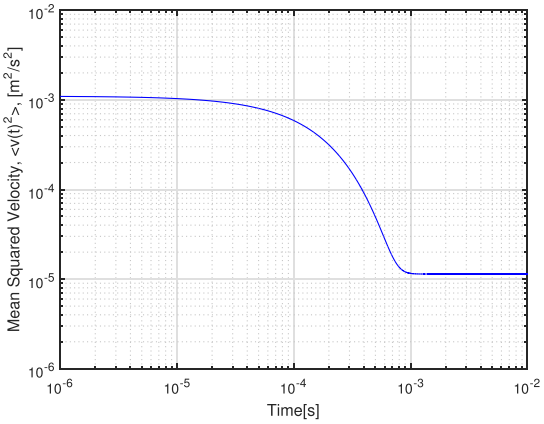

Fig. 5. Mean squared velocity, $< v(t)^2 >$, of intra-body particles (red blood cells in our assumed scenario) versus time.

A. Numerical Analysis

We start by first numerically analyzing the mathematical model presented in Sec. IV. Fig. 3 presents the Johnson-Nyquist noise power spectral density at the high frequency regime including the THz frequency band. We specifically selected a large range of frequencies to understand the receiver impact on the communication link. It can be noticed that noise in electrical resistors has a flat power spectrum; hence, white noise could be easily utilized as a model without compromising accuracy. Although the Johnson-Nyquist noise power spectral density value is small, it is significant in the context of nanonetworks, which rely on the transmission of very weak signals, including low-energy very-short pulses, causing them to be sensitive to noise.

In addition, Planck's function, given in (10), is used to approximate the intra-body background radiation. This noise is stimulated by the temperature of the absorbing molecules, causing the intra-body medium to become a Black-body radiator. Similar to [15], in order to focus on the radiative behavior of the intra-body noise, the antenna effective area is discarded. Thus, we plot the intra-body spectral radiance, E_f, at the THz frequency band as shown in Fig. 4. It is to be noted that the Black-body hemispherical emissive power is π times the Black-body intensity, which should be considered when converting units.

Further, calculating the mean squared velocity, $\langle v(t)^2 \rangle$, presented in Fig. 5, is essential for computing the Doppler-shift-induced noise power spectral density. Actually, Fig. 5 reinforces the "Fluctuation Dissipation Theorem" [39] that expresses the balance between "friction" which tends to drive any system to a completely dead state and "noise" which keeps the system alive. This balance is necessary to maintain a thermal equilibrium state at long times.

In Fig. 6, the Doppler-shift-induced noise power spectral density is presented. Such noise contribution shows how a pure frequency, e.g., a pure sinusoid, which is an impulse in the frequency domain, is spread out across frequency when it passes through the intra-body channel. It is to be noted that the 'bowl shape' is the classic form of this Doppler spectrum. The frequency range where the power spectrum is nonzero defines the Doppler spread. The sharpness of the boundaries of the Doppler spectrum viewed in Fig. 6 are due to the sharp upper limits on the Doppler shift produced by a nano-antenna travelling among the scatterers of the intra-body model. Due to multiple scattering, the incident light may have its direction partly randomized before interacting with red cells, and frequency multiples can be produced by scattering from multiple red cells. Such complex effects preclude exact

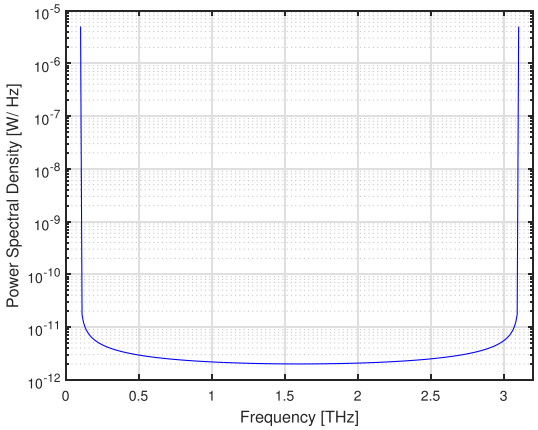

Fig. 6. Doppler shift induced noise power spectral density of an intra-body medium at the THz frequency band.

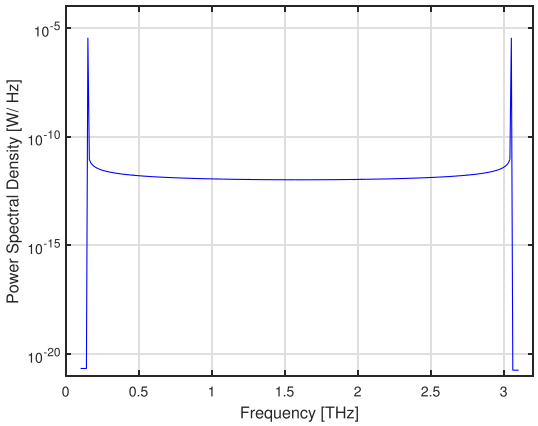

Fig. 7. Total noise power spectral density of an intra-body medium at the THz frequency band.

calculation of the shape of the Doppler spectrum. The overall noise power spectral density is provided in Fig. 7. Since the Doppler shift induced noise constitutes the larger contribution in comparison to the Johnson-Nyquist and Black-body noise, it is noticed that the overall noise power spectral density takes the form of the Doppler spectrum.

B. Model Validation

In contrast to both the Johnson-Nyquist and the Black-body noises, the Doppler-shift induced noise arises due to signal transmission. Thus, in this section, the emphasis will be on verifying the numerical analysis associated with the Doppler effect. To carry out the validation, we compare the motion of a nano-antenna within an ensemble of intra-body particles to the Brownian motion of a microswimmer [52]. Such analogy is conducted as microswimmers are able to propel themselves, exhibiting an interplay between random fluctuations and active swimming. Hence, their Brownian motion captures the stochastic diffusion of particles as they travel through n-dimensional spaces filled with other particles and physical barriers.

An important parameter used to characterize the stochastic behavior of particles is the mean squared velocity, $< \upsilon(t)^2 >$, presented in (29). This value is of ultimate interest as the goal of particle tracking studies is often to define the average velocity of biological motion on a molecular level. However, under most circumstances, the velocity cannot be observed directly in empirical experimentation. A more precise qualitative consideration can be made by simulating the mean square displacement (MSD) of the particle's motion. The MSD quantifies how a particle moves from its initial position, and can be found from a trajectory as [52]

$$MSD(\tau) = \left\langle [x(t+\tau) - x(t)]^2 + [y(t+\tau) - y(t)]^2 \right\rangle, \quad (44)$$

where τ is the timescale for diffusion. Numerically, the MSD can be calculated from a trajectory $[x_n, y_n]$ sampled at discrete times, t_n, with a step size Δt as [52]

$$MSD(\Delta t) = \left\langle (x_{n+m} - x_n)^2 + (y_{n+m} - y_n)^2 \right\rangle. \quad (45)$$

In order to be capable of properly relating the MSD to the particle velocity, one must understand the various modes of motion, namely, normal diffusion, confined diffusion and active transport [53]. In our model, we deal with nano-antennas which are probing the intra-body medium. When a nano-antenna is moving in the direction of the electric force, it accelerates, and its gyro-radius expands. When its moving against the electric force, it decelerates and its gyro-radius contracts. Such distortion of the gyro-radius causes the nano-antenna to drift. As the nano-antenna is moving, the center of each new wavefront is slightly displaced. Consequently, the wave-fronts begin to bunch up and spread further apart, causing the Doppler effect. Superimposed on this motion is the normal diffusion of the intra-body particles, characterized by the diffusion coefficient, D, given in (19). Thus, the active transport relationship between MSD and time will best describe the aforementioned scenario. This relation is given as [53]

$$MSD = \upsilon(t)^2 \Delta t^2 + 4D\Delta t, \quad (46)$$

where υ is the velocity of the directed motion. In this way, the motion of a nano-antenna mimics that of a Brownian particle with inertia. By re-arranging (46) to solve for $\upsilon(t)$ and then taking the average, the mean squared velocity, $< \upsilon(t)^2 >$, can be computed. Fig. 8 shows the MSD of a simulated trajectory of 100 particles (both biological cells and nano-antennas) versus time. The plot of displacement shows that it has a distinct quadratic component. Fig. 9 presents $< \upsilon(t)^2 >$ for each simulation. A thick black line indicates the best overall estimate of $< \upsilon(t)^2 >$ along with error bars in red.

By comparing the results shown in Fig. 9 to those in Fig. 5 over the time interval, $t = 0 : \tau : (N-1) * \tau$, where τ is 1 ms and N is the number of generated samples, one can notice that the values of $< \upsilon(t)^2 >$ are very close. A short time interval is chosen in order to accurately capture the distinct changes in $< \upsilon(t)^2 >$. It is to be observed that the likely error of this measurement decreases as the square root of the number of samples. The significance of this conclusion lies in validating the Doppler-shift-induced noise which is dependent

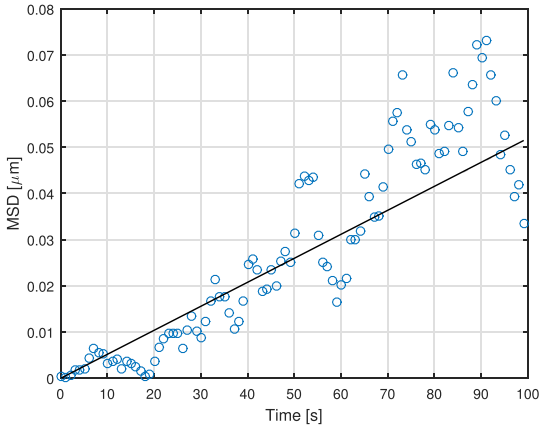

Fig. 8. Simulated MSD for 100 particles. The black line indicates the theoretical MSD value.

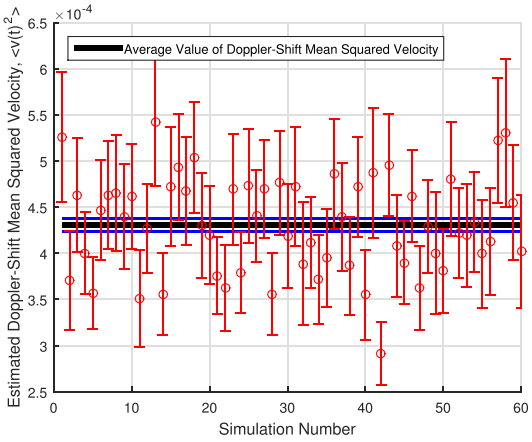

Fig. 9. Estimated mean squared velocity, $< v(t)^2 >$, with error bars in red. The thick black line indicates the best overall estimate of $< v(t)^2 >$. The number of generated simulations N is 60.

on the signal transmission and hence has the major impact on intra-body communication in the THz frequency band.

VI. Conclusion

The progress witnessed in the areas of nano-electronics, nano-photonics, and wireless communication is opening the door towards advanced healthcare networks, namely, in-vivo Wireless Nanosensor Networks (iWNSNs). As we are at the verge of such medical revolution, it is the utmost time to study the reliability of the communication link interconnecting nanosensors. In previous studies, propagation models accounting for intra-body signal losses in the THz frequency band have been presented. In this paper, a stochastic noise model for intra-body systems operating in the THz frequency band has been developed. The identified noise sources include the Johnson-Nyquist noise, Black-body noise as well as the Doppler-shift-induced noise. A comprehensive analysis illustrating the physical fundamentals associated with each noise source along with the derivation of the probability distribution of each noise component has been presented. Consequently, the total noise power-spectral density of the iWNSN in the THz frequency band was computed. It has been concluded that the Doppler-shift-induced noise has the larger impact in comparison to both the Johnson and Black-body noises. The model has been validated via two-dimensional particle simulations as our presented framework resembles the active transport motion of particles. The importance of the presented framework lies in understanding the underlying environment through which wireless communication will be initiated. It will aid in identifying the number of received bits that have been altered due to noise, interference, distortion or bit synchronization. Thus, the proposed model will extend the application scope of nano-networks, guide the development of practical communication strategies among intra-body nanosensors, as well as simulate our understanding of cellular processes and drug carriers in inertial micro-fluidic devices.

References

[1] T. Li *et al.*, "Highly efficient freestyle magnetic nanoswimmer," *Nano Lett.*, vol. 17, no. 8, pp. 5092–5098, 2017.
[2] H. Kim and M. J. Kim, "Electric field control of bacteria-powered microrobots using a static obstacle avoidance algorithm," *IEEE Trans. Robot.*, vol. 32, no. 1, pp. 125–137, Feb. 2016.
[3] T. Ding *et al.*, "Light-induced actuating nanotransducers," *Proc. Nat. Acad. Sci. USA*, vol. 113, no. 20, pp. 5503–5507, 2016.
[4] P. Miao *et al.*, "Orbital angular momentum microlaser," *Science*, vol. 353, no. 6298, pp. 464–467, Jul. 2016.
[5] M. Nafari and J. M. Jornet, "Modeling and performance analysis of metallic plasmonic nano-antennas for wireless optical communication in nanonetworks," *IEEE Access*, vol. 5, pp. 6389–6398, 2017.
[6] J. M. Jornet and I. F. Akyildiz, "Channel modeling and capacity analysis for electromagnetic wireless nanonetworks in the terahertz band," *IEEE Trans. Wireless Commun.*, vol. 10, no. 10, pp. 3211–3221, Oct. 2011.
[7] M. A. Eckert *et al.*, "Novel molecular and nanosensors for *in vivo* sensing," *Theranostics*, vol. 3, no. 8, p. 583, 2013.
[8] I. F. Akyildiz, F. Brunetti, and C. Blázquez, "Nanonetworks: A new communication paradigm," *Comput. Netw.*, vol. 52, no. 12, pp. 2260–2279, 2008.
[9] K. Yang, A. Pellegrini, M. Munoz, A. Brizzi, A. Alomainy, and Y. Hao, "Numerical analysis and characterization of THz propagation channel for body-centric nano-communications," *IEEE Trans. THz Sci. Technol.*, vol. 5, no. 3, pp. 419–426, May 2015.
[10] H. Q. Abbasi, H. El Sallabi, N. Chopra, K. Yang, K. A. Qaraqe, and A. Alomainy, "Terahertz channel characterization inside the human skin for nano-scale body-centric networks," *IEEE Trans. THz Sci. Technol.*, vol. 6, no. 3, pp. 427–434, May 2016.
[11] K. Yang, A. Pellegrini, A. Brizzi, A. Alomainy, and Y. Hao, "Numerical analysis of the communication channel path loss at the THz band inside the fat tissue," in *Proc. Microw. Workshop Ser. RF Wireless Technol. Biomed. Healthcare Appl. (IMWS-BIO)*, Dec. 2013, pp. 1–3.
[12] H. Elayan, R. M. Shubair, J. M. Jornet, and P. Johari, "Terahertz channel model and link budget analysis for intrabody nanoscale communication," *IEEE Trans. Nanobiosci.*, vol. 16, no. 6, pp. 491–503, Sep. 2017.
[13] H. Elayan, R. M. Shubair, J. M. Jornet, and R. Mittra, "Multi-layer intrabody terahertz wave propagation model for nanobiosensing applications," *Nano Commun. Netw.*, vol. 14, pp. 9–15, Dec. 2017.
[14] P. Johari and J. M. Jornet, "Nanoscale optical wireless channel model for intra-body communications: Geometrical, time, and frequency domain analyses," *IEEE Trans. Commun.*, vol. 66, no. 4, pp. 1579–1593, Apr. 2017.
[15] J. Kokkoniemi, J. Lehtomäki, and M. Juntti, "A discussion on molecular absorption noise in the terahertz band," *Nano Commun. Netw.*, vol. 8, pp. 35–45, Jun. 2016.
[16] G. Piro, K. Yang, G. Boggia, N. Chopra, L. A. Grieco, and A. Alomainy, "Terahertz communications in human tissues at the nanoscale for healthcare applications," *IEEE Trans. Nanotechnol.*, vol. 14, no. 3, pp. 404–406, May 2015.
[17] R. Zhang, K. Yang, A. Alomainy, Q. H. Abbasi, K. Qaraqe, and R. M. Shubair, "Modelling of the terahertz communication channel for *in-vivo* nano-networks in the presence of noise," in *Proc. 16th Medit. Microw. Symp. (MMS)*, Nov. 2016, pp. 1–4.

[18] F. Li, W. Liu, C. Stefanini, X. Fu, and P. Dario, "A novel bioinspired PVDF micro/nano hair receptor for a robot sensing system," *Sensors*, vol. 10, no. 1, pp. 994–1011, 2010.

[19] H. Elayan, P. Johari, R. M. Shubair, and J. M. Jornet, "Photothermal modeling and analysis of intrabody terahertz nanoscale communication," *IEEE Trans. Nanobiosci.*, vol. 16, no. 8, pp. 755–763, Dec. 2017.

[20] Y. Feldman, Y. A. Gusev, and M. Vasilyeva, "Dielectric relaxation phenomena in complex systems," Dept. Inst. Phys., Kazan Federal Univ., Kazan, Russia, Tech. Rep., 2012, p. 134.

[21] K. M. Yaws, D. G. Mixon, and W. P. Roach, "Electromagnetic properties of tissue in the optical region," *Proc. SPIE*, vol. 6435, pp. 643507, Feb. 2007.

[22] J. Xu, K. W. Plaxco, and S. J. Allen, "Absorption spectra of liquid water and aqueous buffers between 0.3 and 3.72 THz," *J. Chem. Phys.*, vol. 124, no. 3, p. 36101, 2006.

[23] J. T. Kindt and C. A. Schmuttenmaer, "Far-infrared dielectric properties of polar liquids probed by femtosecond terahertz pulse spectroscopy," *J. Phys. Chem.*, vol. 100, no. 24, pp. 10373–10379, 1996.

[24] C. B. Reid, G. Reese, A. P. Gibson, and V. P. Wallace, "Terahertz time-domain spectroscopy of human blood," *IEEE Trans. THz Sci. Technol.*, vol. 3, no. 4, pp. 363–367, Jul. 2013.

[25] K. Yang, N. Chopra, Q. Abbasi, K. Qaraqe, and A. Alomainy, "Collagen analysis at terahertz band using double-debye parameter extraction and particle swarm optimisation," *IEEE Access*, vol. 5, pp. 27850–27856, 2017.

[26] P. Malik, V. Katyal, V. Malik, A. Asatkar, G. Inwati, and T. K. Mukherjee, "Nanobiosensors: Concepts and variations," *ISRN Nanomater.*, vol. 2013, Aug. 2013, Art. no. 327435.

[27] D. L. Woolard, W. R. Loerop, and M. S. Shur, *Terahertz Sensing Technology: Emerging Scientific Applications & Novel Device Concepts*, vol. 2. Singapore: World Scientific, 2004.

[28] A. B. Carlson, *Communication Systems: An Introduction to Signals and Noise in Electrical Communication* (McGraw-Hill Series in Electrical and Computer Engineering). New York, NY, USA: McGraw-Hill, 1986. [Online]. Available: https://books.google.ae/books?id=V_JSAAAAMAAJ

[29] B. M. Oliver, "Thermal and quantum noise," *Proc. IEEE*, vol. 53, no. 5, pp. 436–454, May 1965.

[30] M. Planck, *The Theory of Heat Radiation*. Chelmsford, MA, USA: Courier Corporation, 2013.

[31] J. R. Howell, M. P. Mengü, and R. Siegel, *Thermal Radiation Heat Transfer*. Boca Raton, FL, USA: CRC Press, 2010.

[32] S. Varró, "Irreducible decomposition of Gaussian distributions and the spectrum of black-body radiation," *Phys. Scripta*, vol. 75, no. 2, p. 160, 2007.

[33] S. Varró, "The digital randomness of black-body radiation," *J. Phys. Conf. Ser.*, vol. 414, no. 1, p. 012041, 2013.

[34] W. Feller, *An Introduction to Probability Theory and its Applications*, vol. 2. Hoboken, NJ, USA: Wiley, 2008.

[35] C. V. Heer, *Statistical Mechanics, Kinetic Theory, and Stochastic Processes*. Amsterdam, The Netherlands: Elsevier, 2012.

[36] E. Frey and K. Kroy, "Brownian motion: A paradigm of soft matter and biological physics," *Annalen Physik*, vol. 14, nos. 1–3, pp. 20–50, 2005.

[37] R. Kubo, "The fluctuation-dissipation theorem," *Reports Progr. Phys.*, vol. 29, no. 1, p. 255, 1966.

[38] L. Sjögren. *Lecture Notes Stochastic Processes*. [Online]. Available: http://physics.gu.s frtbm/joomla/media/mydocs/LennartSjogren/kap6.pdf

[39] R. Zwanzig, *Nonequilibrium Statistical Mechanics*. London, U.K.: Oxford Univ. Press, 2001.

[40] S. O. Rice, "Mathematical analysis of random noise," *Bell Syst. Tech. J.*, vol. 23, no. 3, pp. 282–332, 1944.

[41] M. J. Gans, "A power-spectral theory of propagation in the mobile-radio environment," *IEEE Trans. Veh. Technol.*, vol. VT-21, no. 1, pp. 27–38, Feb. 1972.

[42] B. Eisenberg and R. Sullivan, "Why is the sum of independent normal random variables normal?" *Math. Mag.*, vol. 81, no. 5, pp. 362–366, 2008.

[43] H. Guo, P. Johari, J. M. Jornet, and Z. Sun, "Intra-body optical channel modeling for *in vivo* wireless nanosensor networks," *IEEE Trans. Nanobiosci.*, vol. 15, no. 1, pp. 41–52, Jan. 2016.

[44] T. Uppal and R. Mogra, "RBC motion and the basis of ultrasound doppler instrumentation," *Australas. J. Ultrasound Med.*, vol. 13, no. 1, pp. 32–34, 2010.

[45] J. G. Kiang, J. A. Ives, and W. B. Jonas, "External bioenergy-induced increases in intracellular free calcium concentrations are mediated by na^{+}/ca^{2+} exchanger and l-type calcium channel," *Mol. Cellular Biochem.*, vol. 271, nos. 1–2, pp. 51–59, 2005.

[46] I. Ignatov, O. Mosin, and C. Stoyanov, "Fields in electromagnetic spectrum emitted from human body. applications in medicine," *J. Health, Med. Nursing*, vol. 7, nos. 1–22, pp. 1–23, 2014.

[47] L. Miccio, P. Memmolo, F. Merola, P. Netti, and P. Ferraro, "Red blood cell as an adaptive optofluidic microlens," *Nature Commun.*, vol. 6, p. 6502, Mar. 2015.

[48] X. Ren, P. Ghassemi, H. Babahosseini, J. S. Strobl, and M. Agah, "Single-cell mechanical characteristics of human breast cell lines analyzed by multi-constriction microfluidic channels," in *Proc. AACR Annu. Meeting*, 2017, p. 3924.

[49] M. Diez-Silva, M. Dao, J. Han, C.-T. Lim, and S. Suresh, "Shape and biomechanical characteristics of human red blood cells in health and disease," *MRS Bull.*, vol. 35, no. 5, pp. 382–388, 2010.

[50] J. W. Prothero, *The Design of Mammals*. Cambridge, U.K.: Cambridge Univ. Press, 2015.

[51] Viscopedia. *A Free Encyclopedia for Viscosity*. [Online]. Available: http://www.viscopedia.com/viscosity-tables/substances/whole-blood

[52] G. Volpe, S. Gigan, and G. Volpe, "Simulation of the active brownian motion of a microswimmer," *Amer. J. Phys.*, vol. 82, no. 7, pp. 659–664, 2014.

[53] N. Ruthardt, D. C. Lamb, and C. Bräuchle, "Single-particle tracking as a quantitative microscopy-based approach to unravel cell entry mechanisms of viruses and pharmaceutical nanoparticles," *Mol. Therapy*, vol. 19, no. 7, pp. 1199–1211, 2011.